Ninth International Conference on CFD in the Minerals and Process Industries
CSIRO, Melbourne, Australia
10-12 December 2012

INVESTIGATION OF DROPLET EVAPORATION IN A BUBBLING FLUIDIZED BED

Subhasish Mitra, Mayur J. Sathe, Elham Doroodchi, Geoffrey M. Evans*
Discipline of Chemical Engineering, School of Engineering, University of Newcastle, NSW 2308, AUSTRALIA
[1]*Corresponding author, E-mail address: Geoffrey.Evans@newcastle.edu.au

ABSTRACT

Droplet evaporation in fluidized beds is of great interest in applications like fluidized catalytic cracking units. Although a significant number of analyses are available for modelling of droplet vaporization in a fluidized bed, very little work has been performed experimentally to measure the vapour concentration followed by numerical validation. In the present work, acetone droplet evaporation in a bubbling fluidized bed is studied experimentally as well as numerically. A liquid jet of acetone is injected into a hot bubbling fluidized bed kept well above saturation temperature of acetone. Non-intrusive Schlieren imaging, based on the difference in refractive index, is used to trace the acetone vapour concentration profile. The bubbling fluidized bed is modelled in an Eulerian framework using a simplistic porous media approach while the droplets are modelled in a Lagrangian framework. Intense interactions are observed between the evaporating droplets and hot particles during contact with re-suspension of particles. Experimental measurement and CFD results and measured vapour concentration are compared and found to be in qualitative agreement.

Keywords: bubbling fluidized bed, droplet, evaporation, CFD, Schlieren imaging.

NOMENCLATURE

a_p particle surface area
C_p heat capacity
d_p particle diameter
g gravitational constant
k_{th} thermal conductivity
$k_{th,t}$ turbulent thermal conductivity
m mass of particle
M_w molecular weight
P pressure
R universal gas constant
t time
T_p particle temperature
u velocity
y mole fraction
ρ density
μ dynamic viscosity
ε_b bed porosity
Φ particle sphericity
λ latent heat of vaporization

Dimensionless number:

Nu Nusselt number
Pr Prandtl number
Re Reynold number
Sc Schmidt number
Sh Sherwood number

INTRODUCTION

Heat transfer mechanisms in a gas solid fluidized bed can be broadly classified into two categories, namely: homogeneous and heterogeneous (Martin, 1990). In homogeneous mode, heat is assumed to be transferred purely by convection from the surrounding gas to the evaporating droplets. Infinite thermal conductivity is often assumed which ignores any temperature gradient inside the droplet (Martin, 1990; Buchanan, 1994). Heat transfer to the droplet during its lifetime is considered to occur in two distinct modes: (1) preheating of the liquid to its boiling temperature without vaporization; and (2) vaporization at constant temperature (Buchanan, 1994). Vaporization time is strongly dependent on droplet diameter which increases significantly with increase in droplet size (Martin, 1990; Buchanan, 1994; Mirgain et al., 2001; Leclere et al., 2004). In heterogeneous vaporization, droplets are considered to undergo collision with solid particles. Both heat and mass transfer phenomena are largely governed by this collision process (Nayak et al., 2005; Li et al, 2010; Pougatch et al., 2012). Conduction dominates the heat transfer process during contact when droplets are large enough compared to the catalyst particles (Martin, 1990). Leidenfrost effect is considered at the contact surface of droplet and hot solid particles which reduces the heat transfer coefficient (Buchanan et al., 1994; Nayak et al., 2005). Interactions of droplets and hot particles show interesting phenomena like vapour explosion, resuspension of particles and agglomerate formation. Whilst first two phenomena were reported to be dependent primarily on thermal properties of the liquids (Gehrke et al., 2009), the latter phenomenon was attributed to a critical droplet size (Leclere et al., 2004). A comprehensive numerical analysis of droplet particle interactions in fluidized bed involving heat and mass transfer were reported by Nayak et al, (2005); Li et al., (2010); Behjat et al., (2011) and Pougatch et al., (2012). Although vaporization time, flow pattern (Fan et al., 2001), and temperature profile (Wang et al., 2003) of an evaporating jet in a gas-solid fluidized bed have been widely investigated, not much is reported about evaporation phenomena in bubbling fluidized bed. For this reason, the focus of this study is on quantifying, the vapour concentration profile resulting from liquid jet impinging on a hot bubbling fluidized bed, both experimentally and theoretically.

EXPERIMENTAL SET-UP

A schematic of the experimental setup is presented in Figure 1. A circular (45 mm ID) borosilicate glass fluidized bed of height 45 mm fitted with a sintered ceramic gas distributor was filled with glass ballotini particles (D_{43} = 228 μm). The particles can be classified as overlap between Geldart A and B categories. Particle size

distribution was determined using a MALVERN particle size analyser. A 200W cartridge heater was immersed into the bed. A 1 mm diameter 'T' type thermocouple was inserted into the bed for temperature measurement. The Schlieren imaging (Kelly-Zion et al., 2009) system comprised of a large focal length (f = 6D) 200 mm diameter (D) concave mirror, light source, knife edge and a high speed camera. The mirror was mounted on a vibration resistant aluminium frame. A microscope arc lamp (12VDC) was used as the light source. The lamp was placed at the focal length of the mirror. A knife edge was positioned on a traverse at this focal point before a CMOS camera (Dantec IDT) fitted with 100 mm focal length lens (Nikon). Brightness and contrast of the image was controlled adjusting the knife edge position by cutting the incident light ray on camera. The fluidized bed set-up

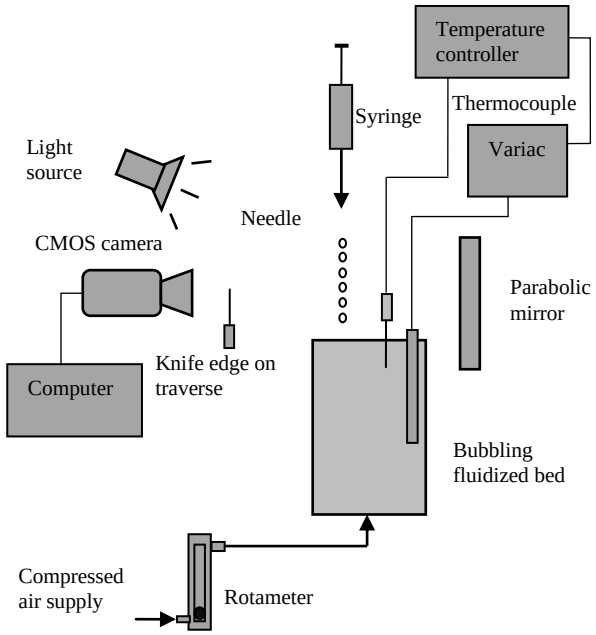

Figure 1: Experimental setup for Schlieren imaging of vapour concentration in a bubbling fluidized bed

was placed closed to the mirror and covered from all sides to prevent unwanted air draft. At start-up, the air flow was set between 2.5-3.0 L/min to maintain a bubbling state. This ensured that the bed was well mixed during the heating-up period. After reaching the set point temperature of 150^0C, air flow rate was then reduced to 1.5 L/min to maintain a minimum bubbling condition. Eruption of few bubbles occurred at the bed surface while most of the bed remained almost stationary. After steady state temperature was reached, 0.2 ml AR grade acetone was injected manually using a 1 ml syringe fitted with 20 gauge needle onto the top of the fluidized bed and images were captured at the same time. The concentration of acetone was calculated from the images based on separate calibration measurements. This calibration data were obtained by measuring image intensity of a pure acetone vapour jet.

COMPUTATIONAL MODEL

A three dimensional Eulerian-Lagrangian model involving a gas phase and droplet phase was used to model acetone liquid jet impingement on bubbling fluidized bed. A separate three dimensional Eulerian model was used to model acetone vapour jet. The continuity equation can be written as follows,

$$\frac{\partial \rho}{\partial t} + \nabla.(\rho u) = 0 \quad (1)$$

Momentum equation with source term (S_m) is given as,

$$\frac{\partial \rho u}{\partial t} + \nabla.(\rho u u) = -\nabla p + \nabla.\mu(\nabla u + \nabla u^T) + S_m. \quad (2)$$

A simplistic porous media concept was applied to model the presence of the solid phase. This approach was adopted in lieu of kinetic theory of granular flow since most of solid particles remained stationary with low gas hold up and negligible solid dispersion at the minimum bubbling state. The viscous and inertial resistance required to model porous media appear as the negative source terms in the momentum equation and can be written as:

$$\boldsymbol{S_m = -\left(\alpha u + \beta \frac{1}{2}\rho |u| u\right)} \quad (3)$$

where α and β are the viscous and inertial resistance respectively and calculated comparing Eq.3 with Eq.4. Eq. 4 is the well known Ergun (1952) equation where coefficients A and B take different values based on the nature of the particles and operating conditions. In the present work, values of 150 and 1.75 were considered for A and B. The porous media was considered to be isotropic which rendered these momentum source terms equal in all three directions.

$$\frac{dP}{dx} = A\frac{\mu(1-\varepsilon_b)^2}{\Phi^2 d_p^2 {\varepsilon_b}^3}u + B\frac{\rho(1-\varepsilon_b)}{\Phi d_p {\varepsilon_b}^3}u^2 \quad (4)$$

The energy equation can be written as, (5)

$$\frac{\partial(\rho E)}{\partial x} + \nabla.[u(\rho E + p)] = \nabla.\left[\left(k_{th} + k_{th,t}\right)\nabla T\right] + S_e$$

where S_e is a source term.

The species transport equation was used to model concentration of acetone vapour,

$$\boldsymbol{\frac{\partial(\rho y_i)}{\partial x} + \nabla.(\rho u y_i) = -\nabla.J_i + S_i} \quad (6)$$

where flux J of i^{th} component in the mixture having mole fraction y is given by:

$$J_i = -(\rho D_i + \frac{\mu_t}{Sc_t})\nabla y_i \quad (7)$$

and D_i is the diffusivity of the i^{th} component in the mixture, μ_t is turbulent diffusivity, Sc_t is turbulent Schmidt number and y_i is the mole fraction and S_i is the source term for i^{th} component in the mixture respectively.

Although the fluidized bed was operated in laminar regime, the freeboard portion over the bed indicated clearly turbulent flow field in the experiment due to large temperature difference. Moreover impact of liquid acetone jet caused sudden release of vapour which also added turbulence to the flow field. A two equation RNG k-ε model was therefore used which is suitable for low Reynolds number system. A Large Eddy Simulation (LES) model to account for turbulence was used to simulate the acetone vapour jet. Details of these turbulence models can be found in Ansys Fluent theory guide (2011). Boundary conditions were specified using turbulence intensity (I) and hydraulic radius, where turbulence intensity is obtained by the following equation,

$$I = 0.16Re^{-1/8} \quad (8)$$

The liquid jet was modelled by the Lagrangian approach using Discrete Particle Model (DPM) of FLUENT where the jet is considered to be made of several mono-sized droplets. Coalescence and break-up of the droplets were

not considered in the present work. In the force balance model for the individual liquid droplet, two forces were considered – drag force and buoyant force. The drag force F_d on the droplet is given by:

$$F_d = \frac{18\mu}{\rho_p d_p^2}\left(\frac{C_d Re}{24}\right) \quad (9)$$

where drag coefficient C_d is obtained from following equations,

$$C_d = 0.424 \text{ when Re} > 1000 \quad (10)$$

$$C_d = \frac{24}{Re}\left(1 + \frac{1}{6}Re^{\frac{2}{3}}\right) \text{ when Re} < 1000. \quad (11)$$

Due to high vapour pressure of acetone, vaporization of the liquid jet was assumed to occur involving both mass and heat transfer effects. The rate of mass transfer was modelled by relating the flux of the droplet vapour into gas phase to the gradient of vapour concentration between the droplet surface and bulk gas. The following equations were used:

$$N_i = k_c(C_{i,sat} - C_\infty) \quad (12)$$

$$C_{i,sat} = \frac{P_{sat}(T_p)}{RT_p} \quad (13)$$

where N_i is the mass transfer flux and C_{sat} and C_∞ are the saturation and bulk concentration respectively. k_c is the mass transfer coefficient which was calculated from the Ranz-Marshall (1952) correlation:

$$C_\infty = \frac{y_{i,\infty}P_\infty}{RT_\infty} \quad (14)$$

$$Sh = \frac{k_c d_p}{D_{I,m}} = 2.0 + 0.6Re_p^{0.5}Sc^{0.33} \quad (15)$$

Change in the mass of droplet due to mass transfer with time was computed using:

$$m_p(t + \Delta t) = m_p(t) - N_i a_p M_{w,i}\Delta t \quad (16)$$

Finally, the temperature of the droplet (T_p) was calculated by applying a heat balance:

$$m_p c_p \frac{dT_p}{dt} = ha_p(T_\infty - T_p) + \frac{dm_p}{dt}h_{fg} \quad (17)$$

The heat transfer coefficient *h* was calculated in a similar way using Eq. 15 replacing *Sh* with *Nu*.

When the liquid jet impacts on the particle surface, the droplets motion ceases. This "no slip" condition on the solid surface was implemented by a user defined function (UDF). Since droplets come to rest after impacting on the surface, convection no longer governs the heat transfer and it is reasonable to assume that conduction dominates this phase of heat transfer process. The droplets upon impact on the hot solid particles form a thin layer of vapour film (Buchanan, 1994, Ge et al.,2005) at the contact surface. Considering all the heat transferred to droplet through this vapour layer is used for vaporization, the following heat balance equation can be written:

$$-k_v a_p(T_b - T_p)/l = \dot{m}\lambda \quad (18)$$

where T_b is the bed temperature, k_v is vapour thermal conductivity, $\dot{m}$ is evaporation rate and l is the vapour layer thickness reported to be in the range of 5-20 µm (Ge et al., 2005). A value of 10 µm was assumed in the present work. This custom heat transfer law was activated through a user defined switch function when droplets impinge on the solid particle surface. Second order upwind scheme was used for all variables except pressure which was discretized using standard scheme. Pressure velocity coupling was achieved using SIMPLE algorithm. Gas phase density was calculated using incompressible ideal gas law. Temperature dependent physical properties of fluids were used in the simulations. To achieve close interactions through mass, momentum and energy source terms, a two-way coupling was used between the two phases. In two-way coupling, the Eulerian phase interacts with Lagrangian phase by drag force and turbulence. Lagrangian phase, on the other hand influences the Eulerian phase by exchanging mass, momentum and energy. Convergence of continuous phase after inclusion of all these source terms is ensured by suitably adjusting number of continuous phase iterations per discrete phase iteration.

Mesh and boundary conditions

CFD simulations were performed using the general purpose commercial finite volume code ANSYS FLUENT. Two 3D meshes were prepared in GAMBIT. To keep the computational time reasonable, a cell size of 1mm was used to keep the accuracy of the result within an acceptable limit. To simulate the jet, a cylindrical domain of diameter 43 mm and height 96 mm was chosen containing 3,48,296 hexahedral cells. The bubbling bed computational domain had a diameter of 45 mm and height of 170 mm and contained 3,00,220 hexahedral cells. Figure 2 shows these two computational domains along with the boundary conditions used.

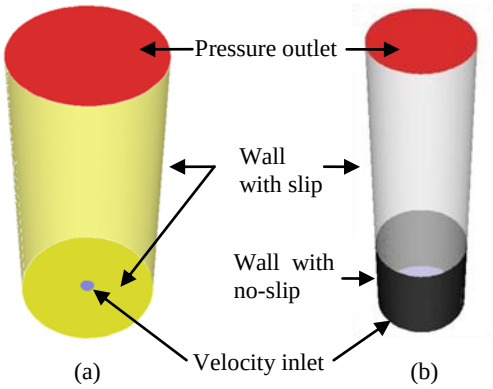

Figure 2: Computational domain and boundary conditions of a) acetone vapour jet and b) fluidized bed simulation cases

Operating and boundary conditions used in simulations are listed below in Table-1.

Table 1: Operating and boundary conditions

Variables	Values
Bed void fraction	0.5
BCs for vapour jet simulations	Inlet velocity : 1.12 m/s Inlet temp : 329 K Outlet pressure : Atm
BCs for bubbling fluidized bed simulations	Inlet velocity :0.0157 m/s Inlet temp : 423 K Outlet pressure : Atm Bed wall temp : 423 K
BCs for DPM simulations	Droplet size : 0.002 m Mass flow rate : 2.145e-04 kg/s

RESULTS

Impingement of the acetone jet on the hot bubbling fluidized bed was captured with high speed camera. Transient vaporization behaviour of these phenomena has been presented in Figure 3. Figure 3a indicates impact of jet on the solid particles. The jet penetrates the bed and comes into contact with more hot solid particles due to increasing temperature gradient towards the bottom of the bed due to presence of the heating element. The liquid jet dissipates kinetic energy while colliding with the solid particles. This results into breakup of the liquid jet into multiple smaller droplets. Smaller droplets evaporate instantaneously with fast release of vapour which resuspends the solid particles around the jet (Figure 3b). Figures 3c-d show multiple droplets generated due to break up of the jet. Some of these droplets coalesce (Figure 3e) and form large droplet (Figure 3f). These large droplets levitate due to generation of a thin vapour film at the contact region with hot particles. After rebounding, such droplets settle down and dissipate their kinetic energy by spreading to form a disc shape structure (Figure 3g). These droplets after repetitive spreading and recoiling finally come to a sessile state. They stay on the bed longer while shrinking in size until completely evaporated. Such large droplets reduce bed surface temperature significantly and form granules (Leclere et al., 2001). Nucleate boiling is observed in all such droplets having clear vapour bubbles inside (Figure 3h).

Image processing

The vapour generated during the liquid jet impact on hot solid particles was quantified using an in-house MATLAB code for image processing. In this process, the pure vapour mass fraction obtained from the acetone jet experiment was used for calibration purposes. Then the time averaged image of the vapour jet was obtained for 1019 image sequences captured over a time span of 2 seconds. Figure 4a shows the instantaneous image of the jet while Figure 4b indicates the time averaged image of the vapour jet. Acetone mass fraction 1.0 was assigned at the jet tip (Figure 4b) with the brightest pixel intensity (255) and 0.0 mass fraction value was assigned to the background outside the jet envelope. A linear calibration curve was therefore obtained with zero intensity corresponding to 100% air or 0% acetone and maximum pixel intensity corresponding to 100% acetone or 0% air. The pixel intensity distribution in the jet image gives mass fraction contour of acetone vapour (Figure 4b). The background contribution from the hot air was eliminated by subtracting the time averaged images of the background prior to acetone injection. This procedure de-noised the subsequent images. Acetone mass fractions from these images were then calibrated using the reference image intensity obtained earlier. In Figure 5, experimentally measured acetone vapour mass fraction has been compared with the simulated result.

In Schlieren imaging, the knife edge blocked some of the refracted lights creating dark patches on the images (Figure 4b). Because of this only the half jet contour (Figure 5a) is shown here. Due to very fine grid requirement for large eddy simulation (LES) which makes the simulation computationally very much expensive, all visible eddies (Figure 4a) could not be resolved. However the simulated vapour concentration profile (Figure 5b) qualitatively agrees with the time averaged experimentally measured vapour contour profile. The concentration of acetone decreases along the length of jet due to gradual diffusion to bulk. This trend is presented in Figure 6.

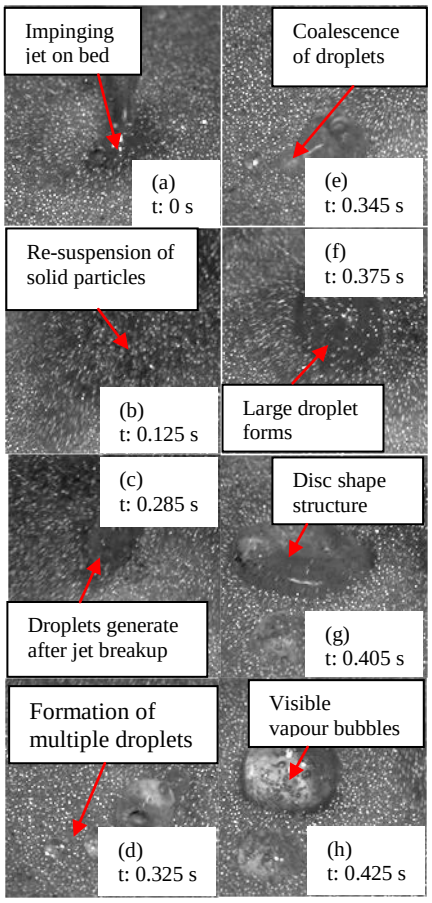

Figure 3: Transient stages of heterogeneous vaporization of the acetone jet in bubbling fluidized bed (1000 fps).

The hot air plume coming out of fluidized bed is turbulent in nature and has visible eddies in it (Figure 7a). Quick vaporization of liquid acetone jet on the hot bed contributes to significant local turbulence. The vapour plume also contains several multiscale eddies. Due to higher refractive index, acetone vapour is distinctly visible from surrounding air (Figure 7b).

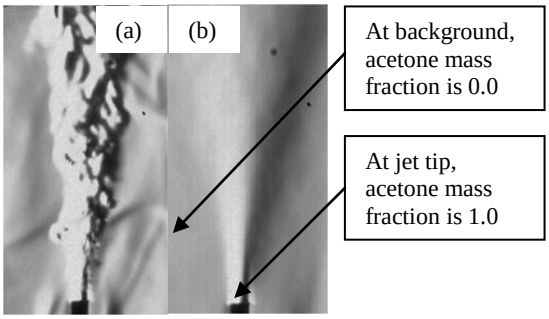

Figure 4: a) image of actual acetone jet and b) time average image used for calibration (500 fps)

An experimental image of liquid acetone jet is shown in Figure 8a. The image is processed (Figure 8b) to remove the background effects as described earlier. Acetone vaporizes at room temperature due to its high vapour pressure. Vapour concentration profile around the jet is

simulated in Figure 8c which qualitatively agrees with the experimental observation.

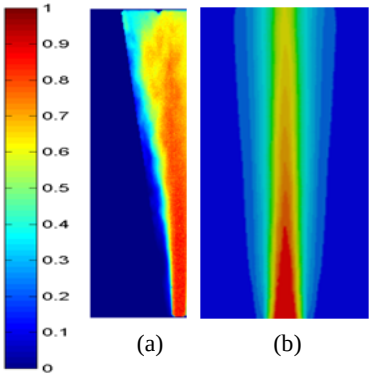

Figure 5: Contour plot of a) experimentally measured acetone vapour concentration profile (half jet shown) b) simulated vapour concentration profile using LES

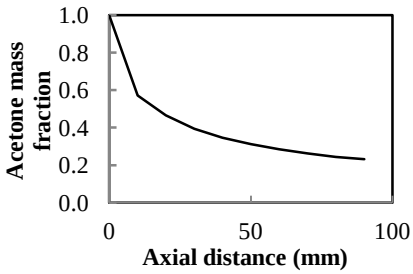

Figure 6: CFD simulation of acetone vapour mass fraction at different radial planes along the jet length

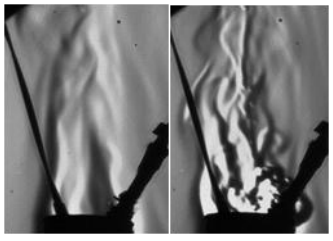

Figure 7: Schlieren image of a) hot air plume over fluidized bed before acetone injection b) distinct plume of acetone vapour over bed after acetone injection (500 fps)

Figures 9a,c,e present mass fractions of acetone vapour at different time instances after injection of liquid acetone jet. CFD simulations (Figures 9b,d,f) indicate generation of acetone vapour with maximum vapour concentration on the bed surface and qualitatively agree with experimental observations. Figure 10 presents generation of acetone vapour with time which reaches a steady value at 9.25s. A deviation of ~ 22% was found in CFD simulation while comparing the mass of liquid acetone injected in the bed and total mass of vapour produced. Although measures were taken to remove the background contribution during image processing, still consistent streaks are observed in Figures 9a,b,c. These disturbances around the impinging jet are attributed to the continuous changing density of background medium due to upward movement of hot air and downward movement of cold air. These circulations due to temperature hence density difference can be seen in the simulated velocity vector plot (Figure 11). Such circulations change the refractive index of the medium causing fluctuations of the background intensity and introduce background noise in the images. The patches in Schlieren images actually show the corresponding positive and negative density gradient of the fluid. These effects made it difficult to completely match simulated results with experimental visualizations. These noises can be eliminated by implementing more rigorous Schlieren system and suitable image processing algorithm. However, qualitatively the simulations capture the vaporization phenomena correctly indicating maximum vapour concentration on the bed surface with diminishing gradient to the bulk.

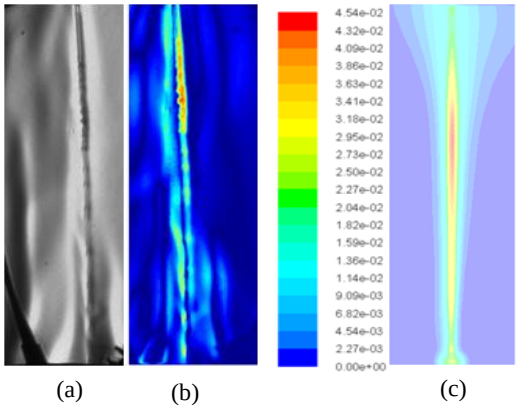

Figure 8: a) Schlieren image of the liquid acetone jet impinging on the fluidized bed (500 fps) b) vapour profile around the jet after image processing c) simulated vapour mass fraction profile

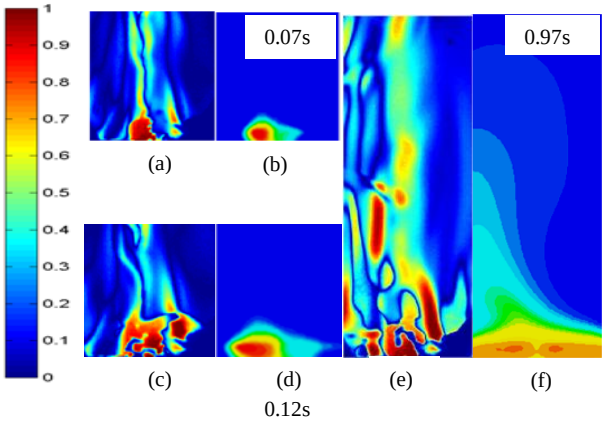

Figure 9: Comparison of vapour mass fractions from Schlieren images and CFD simulations at different time instances after liquid acetone jet impinges on the hot bubbling bed (t = 0 s)

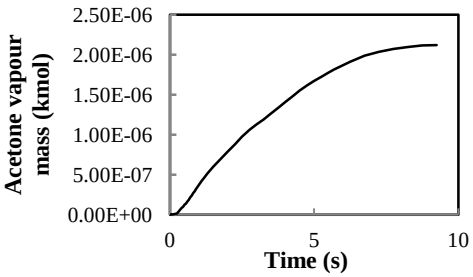

Figure 10: CFD simulation of acetone vapour mass generation during and after impingement of liquid jet on the bubbling fluidized bed

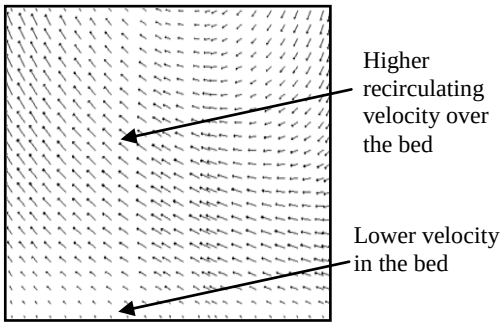

Figure 11: Velocity vector plot (larger vector size indicates higher velocity) shows circulation above the fluidized bed due to temperature difference

The heat transfer process between liquid jet and solid particles during impingement reduces bed temperature. This causes reduction in evaporation rate increasing droplet life on the bed surface and hence possibility of coalescence of droplets and granulation (Leclere et al., 2001). Two-way coupling implemented in the CFD simulations indicate significant reduction temperature at the bed surface (Figure 12a, b).

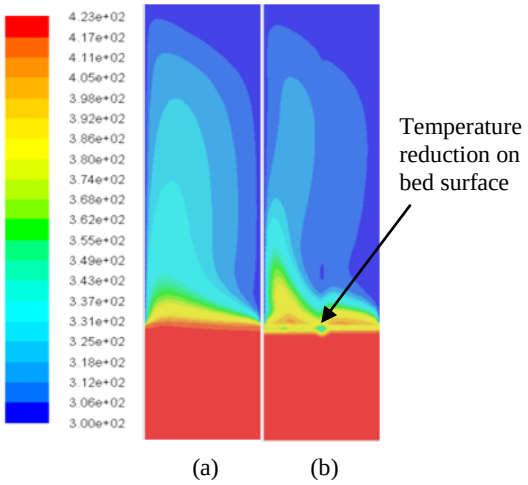

Figure 12: Contour plot of bed temperature a) before acetone injection b) after 1 sec of acetone injection

CONCLUSION

An acetone liquid jet interaction with hot Geldart (A-B) type solid particles in a bubbling fluidized bed involving both homogeneous and heterogeneous evaporation was studied in the present work. Several interesting droplet-particle interaction phenomena like jet breakup to multiple droplets, resuspension of solid particles due to vapour explosion, coalescence of droplets, levitation of droplets, shape deformation of droplets and nucleate boiling of droplets were observed. A vapour concentration measurement technique using Schlieren imaging method along with CFD modelling were presented to quantify heterogeneous vaporization in the bubbling fluidized bed. Based on the difference in refractive index of medium, acetone vapour concentration was measured. The technique could also be used to measure temperature of vapour phase if a correlation between the refractive index and temperature is available. Simulated evaporation phenomenon qualitatively agreed with experimental observations and captured the key features of the vaporization process indicating more vapour concentration on the bed surface and diminishing concentrations in the bulk. Mass balance of injected acetone liquid and vapour produced were found to be within acceptable level of deviation.

ACKNOWLEDGEMENT

The authors gratefully acknowledge the financial support from Australian Research Council (ARC) and British Petroleum (BP), Kwinana, Western Australia to carry out this research work.

REFERENCES

ANSYS FLUENT Theory Guide (2011) Release 14.0.

BUCHANAN, J. S. (1994) "Analysis of heating and vaporization of feed droplets in fluidized catalytic cracking risers", *Ind. Eng. Chem*. Res., 33, 3104-3111.

ERGUN, S., (1952). "Fluid flow through packed columns", *Chem. Eng. Prog.*, 48, 9–94.

FAN L.-S. et al., (2001), "Evaporative liquid jets in gas-liquid-solid flow system", *Chem. Eng. Sci*., 56, 5871 – 5891.

GE, Y.et al., (2005), "Three dimensional simulation of impingement of a liquid droplet on a flat surface in the Leidenfrost regime.", *Physics of Fluids*, 17, 027104.

GEHRKE, S. et al., (2009), "Interaction phenomena between liquid droplets and hot particles—Captured via high speed camera", *Particuology*, 7, 260–263.

KELLY-ZION, L.P. et al., (2009), "Evaporation rates of pure hydrocarbon liquids under the influence of natural convection and diffusion", *Int. J. Heat and Mass Transfer*, 52, 3305 – 3313.

LECLERE, K. et al., (2001), "Liquid vaporization in a fluidized bed", *Ind. Eng. Chem.*, 60, 693-699.

LECLERE, K. et al., (2004), "Experimental measurement of droplet vaporization kinetics", *Chem. Eng. Sci., 60*, 6049- 6066.

MARTIN, M. P. (1990) "Contribution a` l'e´tude des e´le´vateurs de craquage catalytiqu– - Effets lie´s a` l'injection de charge", The`se, INPL, France.

MIRGAIN, C. et al., (2001) "Modelling of feed vaporization in fluid catalytic cracking", *Ind. Eng. Chem*., 39, 4392 – 4399.

NAYAK, S. V. et al., (2005) "Modelling of vaporization and cracking of liquid oil injected in a gas-solid riser", *Chem. Eng. Sci*., 60, 6049-6066.

RANZ, W. E. and MARSHALL, W. R., 1952, "Evaporation from drops", *Chem. Eng. Prog*. 48(3), 141-146 (Part I); 48(4), 173-l 80 {Part II).

WANG, X. et al., (2003), "Concentric evaporative spray jets in dilute gas-solids pipe flows", *Powder Technology*, 129, 59 – 71.

LI, T. et al., (2010), "Numerical modelling of an evaporative spray in a riser", *Powder Technology*, 201, 213 – 229.

BEHJAT, Y. et al., (2011), "Simulation study of droplet vaporization effects on gas-solid fluidized bed", *J. Taiwan Inst. Chem. Eng.*, 42, 419–427.

POUGATCH, K. et al., (2012), "Three-dimensional numerical modelling of interactions between a gas liquid jet and a fluidized bed", *Chem. Eng. Sci.*, 68, 258–277.

